Nuclear Physics B304 (1988) 712–748
North-Holland, Amsterdam

RADIATIVE CORRECTIONS TO BHABHA SCATTERING AT HIGH ENERGIES
(II). Hard photon corrections and Monte Carlo treatment

F.A. BERENDS and R. KLEISS

Instituut-Lorentz, Leiden, The Netherlands

W. HOLLIK

II. Institut für Theoretische Physik, Universität Hamburg, FRG

Received 25 August 1987
(Revised 15 February 1988)

The cross section for single hard photon bremsstrahlung in Bhabha scattering is presented, and its main qualitative features are reviewed. Subsequently, the structure of a Monte Carlo event generator for Bhabha scattering at LEP/SLC energies, including all one-loop electroweak corrections, is discussed, in which the results on the virtual and soft photon corrections, given in the first paper of this set, are incorporated. Finally, a number of numerical results is presented.

1. Introduction

This paper is the second one of a pair dealing with the detailed predictions of the standard model of electroweak interactions [1] in the process of Bhabha scattering. In the first paper (ref. [2], hereafter referred to as I) the phenomenological importance of this process was discussed in some detail. The authors presented expressions for the cross section for

$$e^+(p_+)e^-(p_-) \to e^+(q_+)e^-(q_-), \tag{1.1}$$

in which all one-loop corrections arising in the standard model were included, as well as bremsstrahlung of a soft photon, i.e. with an energy not exceeding a (small) value ΔE. This cross section, which is both ultraviolet and infrared finite, incorporates all "standard" weak effects, and would in principle also be the quantity in which "new-physics effects" in this process [3] are most likely to show up (an exception is the case of the existence of an excited electron, e*, with mass small enough to be produced at a given energy: this would most clearly be seen as an $ee\gamma$ or $ee\gamma\gamma$ event [4]).

0550-3213/88/$03.50

Complete as they are, the results of I are not enough for a successful phenomenological treatment; the effects of hard photon radiation have to be adequately included before a successful prediction is possible. Restricting ourselves to the one-loop level, this means we have to know the cross section for

$$e^+(p_+)e^-(p_-) \to e^+(q_+)e^-(q_-)\gamma(k), \tag{1.2}$$

where the photon has an energy greater than ΔE. Once the ingredients (1.1) and (1.2) are available, we still are not finished; it remains to integrate these cross sections over the phase space admitted by a given experiment. As soon as a 3-body radiative final state is involved this also becomes a highly nontrivial problem. The aim of the present paper is, therefore, threefold. In the first place an expression for the cross section for (1.2) must be presented in a form which is as simple as possible, and its qualitative features must be well understood. Secondly, these results must be combined with those of I in such a way that they can be suitably integrated over phase space: the integration procedure must be both accurate enough so that the one-loop effects can be studied, and flexible enough so that all kinds of experimental restrictions can be imposed on the data. The optimal integration technique seems to be that of Monte Carlo integration by importance sampling, using a multi-channel approach in which each channel is dominant in one kinematical situation. Finally, a number of numerical results are in order; apart from being a reference for checking purposes and an example of the method, these will provide estimates for the radiative corrections which will approximate those made for a very concrete, specific detector set-up. The layout of this paper is as follows. In sect. 2 we discuss the multi-differential hard photon cross section and present an expression valid in all kinematical situations of interest in Bhabha scattering. In sect. 3 we sketch the Monte Carlo approach and draw up a list of ingredients needed for this technique; we subsequently set out to supply all these ingredients. Sect. 4 deals with the cross section (1.1): as will be shown, this is the simplest ingredient from the point of view of Monte Carlo integration. In sect. 5 we discuss the 4 different channels into which the hard photon cross section (1.2) can be split, and in sect. 6 the approximate cross sections valid in the kinematical regions where each of these channels dominate, together with the integrals of these approximate cross sections over the phase space. These results lead directly, in sect. 7, to the derivation of numerical algorithms to generate random values for the various phase-space variables. (Appendix B is devoted to a discussion of the structure of the Monte Carlo program which we have developed with these results.) In sect. 8 we discuss some canonical cuts [5] appropriate for Bhabha scattering, and present numerical results for these cuts.

Finally, a Monte Carlo treatment of mu-pairs can be obtained from the Bhabha case by omitting the t-channel contributions and by introducing muon masses. Such a muon event generator has been constructed.

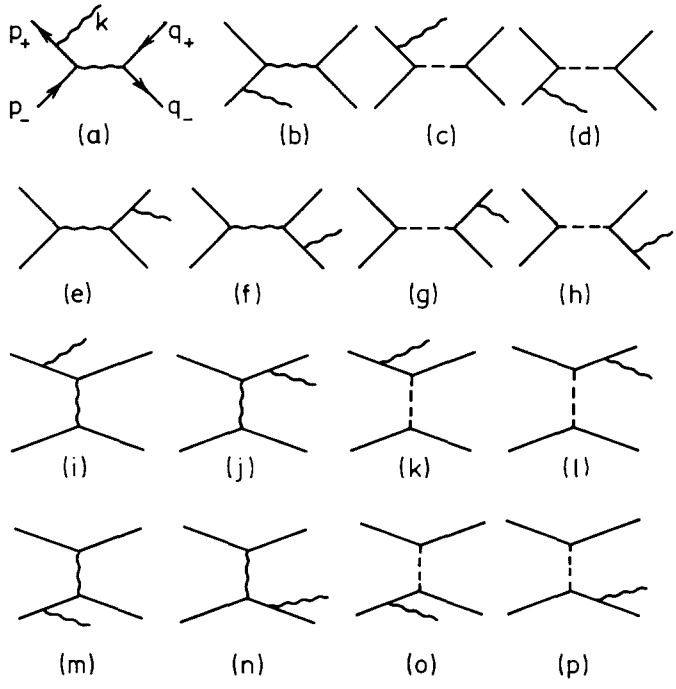

Fig. 1. The sixteen Feynman diagrams contributing to $e^+e^- \to e^+e^-\gamma$ in the Standard Model.

2. The hard photon cross section

In the standard model, the radiative process (1.2) is described by 16 Feynman diagrams, depicted in fig. 1 (as is usual, we neglect the diagrams containing a Higgs boson exchange, and also the $q_\mu q_\nu$ part of the Z^0 propagator; these give contributions that are suppressed by powers of m_e/E). Relatively simple expressions for this cross section, valid in the high-energy limit, have been known for some time. In ref. [6] the first of these was introduced: these results were subsequently further developed by the CALKUL collaboration [7]. Particularly noteworthy is the fact that a factorization of similar nature as to the soft photon limit occurs; the cross section can be written as a slightly generalized form of the nonradiative cross section, multiplied by the well-known "infrared factor" which describes the various infrared and collinear singularities.

In ref. [7] the complete expression for the cross section $e^+e^- \to e^+e^-\gamma$, including a Z^0 with finite width, was given in terms of vector products of the particle momenta. As discussed at length in ref. [8] a better way to handle these processes seems to be to evaluate helicity amplitudes using spinor products. A numerically well-behaved, and very compact form for the amplitudes, and the one we shall use in the following, was given in ref. [8]. In that paper, emphasis was placed on the correct

treatment of the complex phases of the various helicity amplitudes, so that arbitrary beam polarization can be taken into account; here, we shall restrict ourselves to the case of unpolarized beams, and consequently the complex phases are of no importance.

Our expression for the squared matrix element, summed over the final-state spins and averaged over the initial-state spins, is

$$\overline{|M|^2} = \tfrac{1}{4} \sum_{i=1}^{12} |M_i|^2 W_m . \tag{2.1}$$

Here the M_i are the twelve helicity amplitudes which do not vanish in the high-energy limit, and W_m is a factor incorporating the more complicated behaviour in situations where the photon is collinear to one of the fermions. Up to an irrelevant overall complex phase, the M_i are given by

$$\begin{aligned}
M_1 &= u\big[E_{++}(s')v_i + E_{++}(s)v_f + E_{++}(t')v_p + E_{++}(t)v_e\big],\\
M_2 &= u'\big[E_{++}(s')v_i^* + E_{++}(s)v_f^* + E_{++}(t')v_p^* + E_{++}(t)v_e^*\big],\\
M_3 &= t\big[E_{+-}(s')v_i + E_{+-}(s)v_f\big],\\
M_4 &= t'\big[E_{+-}(s')v_i^* + E_{+-}(s)v_f^*\big],\\
M_5 &= s\big[E_{+-}(t')v_p + E_{+-}(t)v_e\big],\\
M_6 &= s'\big[E_{+-}(t')v_p^* + E_{+-}(t)v_e^*\big],\\
M_7 &= s'\big[E_{-+}(t')v_p + E_{-+}(t)v_e\big],\\
M_8 &= s\big[E_{-+}(t')v_p^* + E_{-+}(t)v_e^*\big],\\
M_9 &= t'\big[E_{-+}(s')v_i + E_{-+}(s)v_f\big],\\
M_{10} &= t\big[E_{-+}(s')v_i^* + E_{-+}(s)v_f^*\big],\\
M_{11} &= u'\big[E_{--}(s')v_i + E_{--}(s)v_f + E_{--}(t')v_p + E_{--}(t)v_e\big],\\
M_{12} &= u\big[E_{--}(s')v_i^* + E_{--}(s)v_f^* + E_{--}(t')v_p^* + E_{--}(t)v_e^*\big].
\end{aligned} \tag{2.2}$$

Here, we have introduced the kinematic invariants

$$\begin{aligned}
s &= (p_+ + p_-)^2, \qquad t = (p_+ - q_+)^2, \qquad u = (p_+ - q_-)^2,\\
s' &= (q_+ + q_-)^2, \qquad t' = (p_- - q_-)^2, \qquad u' = (p_- - q_+)^2.
\end{aligned} \tag{2.3}$$

The functions E are the combination of the photon and Z^0 propagator and the electroweak coupling constants

$$E_{\lambda_1\lambda_2}(x) = i\sqrt{8}\left[\frac{e^3}{x} + \frac{e(v-\lambda_1 a)(v-\lambda_2 a)}{x - m_Z^2 + im_Z\Gamma_Z}\right],$$

$$v = a\left(1 - 4\sin^2\theta_w\right), \qquad a = -e/4\sin\theta_w\cos\theta_w, \tag{2.4a}$$

where e denotes the positron electric charge, $\sqrt{4\pi\alpha}$, and m_Z and Γ_Z are the Z^0 mass and total width, respectively; θ_w stands for the electroweak mixing angle. In the notation of I, eq. (2.4a) can be written as

$$E_{\lambda_1\lambda_2}(x) = \frac{ie\sqrt{8}}{x}\sum_i g^{(i)}_{-\lambda_1} g^{(i)}_{-\lambda_2}\chi^{(i)}(x). \tag{2.4b}$$

The quantities $v_{i,f,p,e}$ are the so-called radiation factors, each corresponding to photon bremsstrahlung from a particular fermion line in the diagrams of fig. 1

v_i; initial-state radiation (figs. 1a–d):

$$v_i = s(q_-, q_+)^*/s(k, p_+)s(p_-, k), \tag{2.5a}$$

v_f; final-state radiation (figs. 1e–h):

$$v_f = s(p_+, p_-)^*/s(k, q_-)s(q_+, k), \tag{2.5b}$$

v_p; radiation from the positron line (figs. 1i–l):

$$v_p = s(q_-, p_-)^*/s(k, p_+)s(q_+, k), \tag{2.5c}$$

v_e; radiation from the electron line (figs. 1m–p):

$$v_e = s(p_+, q_+)^*/s(k, q_-)s(p_-, k), \tag{2.5d}$$

where the *spinor product* of two four-momenta p_1^μ and p_2^μ is defined as

$$s(p_1, p_2) = (p_1^y + ip_1^z)\left[\frac{p_2^0 - p_2^x}{p_1^0 - p_1^x}\right]^{1/2} - (p_2^y + ip_2^z)\left[\frac{p_1^0 - p_1^x}{p_2^0 - p_2^x}\right]^{1/2}. \tag{2.6}$$

For a derivation of these formulae we refer the reader to ref. [8]. Up to this point our results are only strictly valid if $m_e = 0$. In order to correctly describe the situations where the photon makes a small angle (of order m_e/E) with one of the

charged fermions, we have introduced the mass effect factor W_m. It reads

$$W_m = \frac{|s(p_+,k)|^2}{2(p_+\cdot k)}\left[1-\frac{m_e^2}{(p_+\cdot k)}\frac{s'(s-s')}{s^2+s'^2}\right]$$
$$\times\frac{|s(p_-,k)|^2}{2(p_-\cdot k)}\left[1-\frac{m_e^2}{(p_-\cdot k)}\frac{s'(s-s')}{s^2+s'^2}\right]$$
$$\times\frac{|s(q_-,k)|^2}{2(q_-\cdot k)}\left[1-\frac{m_e^2}{(q_-\cdot k)}\frac{s(s-s')}{s^2+s'^2}\right]$$
$$\times\frac{|s(q_+,k)|^2}{2(q_+\cdot k)}\left[1-\frac{m_e^2}{(q_+\cdot k)}\frac{s(s-s')}{s^2+s'^2}\right]. \tag{2.7}$$

The effect of this factor is on the one hand to ensure that the cross section peaks in the right places (for not-strictly-massless p^μ, the product $s(p,k)$ vanishes for some k^μ that are not strictly collinear), and on the other hand to take care of the nonleading terms that are suppressed by a factor m_e^2 (this also accounts for those helicity amplitudes that are neglected in the high-energy limit). A more detailed discussion of these points can again be found in ref. [8]. If we evaluate the cross section as indicated above, taking care to handle correctly small values of $p\cdot k$, the result will describe the process (1.2) up to truly negligible terms everywhere in phase space except when s', t or t' are of $O(m_e^2/s)$. The first of these cases will be treated later in this paper; the latter two, corresponding to situations where e^+ or e^- are scattered over angles of order $m_e/E \lesssim 10^{-3}$ degrees, are outside of the scope of this paper: they are, for instance, discussed (in the context of single-photon events) in refs. [9]. The square of the matrix elements can, of course, also be written in a more conventional form, in which no spinor products are involved, but only vector dot-products. This result, which is of course very similar to the one for $e^+e^-\to e^+e^-\gamma$ given in ref. [7], although a bit more systematic and compact, is given for completeness in appendix A.

Now, a short discussion of the phase space is in order. The 5-dimensional phase space element $d\Phi$ is defined as

$$d\Phi = \delta^4(p_+ + p_- - q_+ - q_- - k)\,d^4q_+\,\delta(q_+^2)\,d^4q_-\,\delta(q_-^2)\,d^4k\,\delta(k^2). \tag{2.8}$$

Various choices of phase-space variables can be made; we shall use three different alternatives. First

$$d\Phi = \tfrac{1}{8}\,dq_+^0\,dk^0\,d\Omega_+\,d\phi_a, \tag{2.9a}$$

where q_+^0 is the e^+ energy, Ω_+ its solid angle, and ϕ_a the γ azimuthal angle around

the Ω_+ direction, everything being defined in the lab frame; then,

$$d\Phi = \frac{k^0 q_+^{02}}{2E(E-k^0)}\, dk^0\, d\Omega_\gamma\, d\Omega_+ , \tag{2.9b}$$

where k^0 and Ω_γ are the photon energy and solid angle in the lab frame, and E is the beam energy; finally,

$$d\Phi = \tfrac{1}{16} k^0\, dk^0\, d\Omega_\gamma\, d\Omega_e , \tag{2.9c}$$

where Ω_e is the production solid angle of the e^+, now defined in the centre-of-mass frame of the outgoing e^+e^- pair. Thus, the observable cross section is given by

$$d^5\sigma_{ee\gamma} = \frac{1}{64\pi^5 s}\overline{|M|^2}\, d\Phi . \tag{2.10}$$

Before concluding this section we want to summarize the main qualitative features of the cross section (2.10). These are:

(a) *Infrared peak* – the cross section diverges for $k^0 \to 0$ as $1/k^0$. Since k^0 is defined to be larger than ΔE, which is typically of order 10^{-3}–10^{-2} of E, there is no real singularity; nonetheless the cross section varies over several orders of magnitude as a function of k^0;

(b) *collinear peaks* – if the angle between the photon and any of the $e^\pm$ directions varies from zero to order 1, the cross section changes over typically 10 orders of magnitude (5 orders of magnitude between zero and 0.2 degrees!). This wild behaviour calls for a careful treatment of the photon emission angles;

(c) *low-energy peak* – if the invariant mass of the outgoing e^+e^- pair goes to zero, the s-channel photon propagator blows up; therefore, the photon spectrum is rather wild at its high end as well;

(d) *forward peaks* – as in the nonradiative case, the cross section rises as either the e^+ or e^- scattering angle decreases. In the bremsstrahlung case the cross section in fact remains finite for zero angle; on the other hand the forward peaks for the e^+ and e^- no longer coincide owing to the 3-body kinematics. Although we shall not deal with the zero-angle case here, the cross section increase over 3–4 orders of magnitude in an angular range of 10°–170° again calls for careful treatment.

3. The Monte Carlo approach

We now come to the second part of the problem, namely the integration of the cross section over the allowed phase space. There are two goals which have to be attained. In the first place we want a numerical result for the total cross section, containing as much as possible of the experimental cuts. For the nonradiative cross

section which, due to the 2-body kinematics, depends essentially only on the scattering angle θ, this is a relatively simple problem which can be solved by about every possible numerical integration technique (and possibly even analytically). The radiative cross section varies in four dimensions, rather than one, and behaves wildly, as we have seen. This, together with the necessity of folding in the experimental cuts which are seldom simple in terms of any set of phase-space variables, indicates that our numerical technique has to be that of Monte Carlo integration. In the second place, for purposes of an analysis of the experiments it is desirable to have an *event generator* for our process, which yields events which have the correct distribution, and (a no less important requirement) are independent of one another. In our view the most sensible way to achieve this is to use *importance sampling* [10,11]. Alternative methods, such as the use of antithetic variates, which rely on artificial dependences between subsequent Monte Carlo events, or of stratified sampling, which only works if a minimum number of events is required and their distribution is artificially uniform due to the stratification, seem not to correspond in any simple way to the event-by-event independence, and the statistical fluctuations to be expected, in the actual experiment. Our approach is as follows. The cross section to be integrated consists of the *hard photon cross section* (2.10), taken over H, the allowed phase space for eeγ events, and the *soft photon cross section*

$$\frac{d^2\sigma_{ee}}{d\Omega} = \frac{d\sigma}{d\Omega}(\text{the result of I}), \tag{3.1}$$

defined in the soft region S, i.e. the phase space allowed for elastic ee events. The result for the total cross section can then be written as follows

$$\sigma_{tot} = \int_S \frac{d^2\sigma_{ee}}{d\Omega}\, d\Omega + \int_H \frac{d^5\sigma_{ee\gamma}}{d\phi}\, d\phi. \tag{3.2}$$

The technique of importance sampling now consists of finding a number of (relatively simple) functions $f_i(\phi)$ of the phase space variables such that the hard photon cross section is more or less approximated by a sum of the f_i. The f_i are called the *channels*. In other words, for some α_i the *weight*

$$w(\phi) \equiv \frac{\left(d^5\sigma_{ee\gamma}/d\phi\right)}{\Sigma_i \alpha_i f_i(\phi)}, \qquad \alpha_i > 0, \tag{3.3}$$

should not be too different from a constant over the whole phase space of interest. In our case each f_i describes a different set of the peaks in phase space, and is simple when expressed in different phase-space variables. The numerator in eq. (3.3) is essentially just the matrix element squared, summed and averaged over the spins;

common factors in $d^5\sigma/d\phi$ and the f_i can of course be disregarded. The integral (3.2) can now be rewritten as

$$\sigma_{\text{tot}} = \int_S \frac{d^2\sigma_{ee}}{d\Omega}\, d\Omega + \sum_i \alpha_i \int_H w(\phi) f_i(\phi)\, d\phi . \tag{3.4}$$

Having thus split up the integral in separate pieces we proceed to choose in each integral a particular set of variables ϕ_i which makes the integral simple. We shall use 4 different channels for the hard photon events; we can now interpret the soft photon contribution as a fifth channel, and write

$$\sigma_{\text{tot}} = \sum_{i=1}^{5} \alpha_i \int_{A_i} w(\phi_i) f_i(\phi_i)\, d\phi_i . \tag{3.5}$$

Here, ϕ_5 is the 2-dimensional Ω, and the other ϕ_i are 5-dimensional. A_i is the appropriate integration region in each case, and $f_5(\phi_5) = d^2\sigma_{ee}/d\Omega$ as given in eq. (3.1).

When we choose the $f_i(\phi_i)$ carefully enough, the integrals

$$\sigma_i = \int_{A_i} f_i(\phi_i)\, d\phi_i \tag{3.6}$$

can be calculated, without problems, to great accuracy. Our Monte Carlo approach now consists of the following steps. First, the σ_i are computed under some set of reasonable a priori experimental cuts, such as a minimum scattering angle for the e^+ and e^-. The second step, which can be repeated as often as desired, is the generation of a Monte Carlo event. To this end, first a channel is chosen in a random way, with the probability of channel i being picked equal to

$$P_i = \alpha_i \sigma_i \Big/ \left(\sum_{j=1}^{5} \alpha_j \sigma_j \right). \tag{3.7}$$

Then, a set of random phase space variables ϕ_i is generated by the so-called ith subgenerator such that it is distributed according to the probability density $f_i(\phi_i)/\sigma_i$, finally, the event weight $w(\phi)$ is computed using eq. (3.3). After the desired number N of events has been generated, the exact cross section is estimated to be

$$\sigma_{\text{exact}} = \frac{\Sigma_k w(\phi_k)}{N} \sum_j \alpha_j \sigma_j , \tag{3.8a}$$

where the sum runs over the Monte Carlo events, defined by ϕ_k. The error estimate

on the result is given by [10]

$$\frac{\Delta\sigma_{\text{exact}}}{\sigma_{\text{exact}}} = \frac{1}{\sum_k w(\phi_k)} \left[\sum_k w(\phi_k)^2 - \frac{1}{N} \left(\sum_k w(\phi_k) \right)^2 \right]^{1/2}. \tag{3.8b}$$

A few remarks are in order here. Firstly, in the simulation of experiments it is often desirable to use unweighted events. This can be achieved by applying the following rejection algorithm. Let W_S be the supremum of the weights W, and take a random number ν, equidistributed in $[0,1]$. Then, if $W(\phi_k) > \nu W_S$, accept the Monte Carlo event ϕ_k, else reject it and try the next event. In case W_S is not known beforehand any value larger than the largest observed weight will do. In this way an unbiased sample of events is obtained in which the weights can be taken as unity.

In the second place, the weights $W(\phi_k)$ are only well-behaved if the f_i are chosen carefully enough, so the qualitative features of $d^5\sigma_{ee\gamma}$ are discussed in the previous section will direct our choice of f_i.

In the third place, the a priori weights α_i are in principle arbitrary as long as they are positive; for $N \to \infty$ the Monte Carlo estimate (3.8a) will converge to the true answer for any choice of α_i. For finite N, however, the convergence, depending on the variance of the weight w, will depend on the α_i. This gives us a handle to "tune" the relative strengths of the subgenerators so as to optimize the convergence somewhat. A perhaps more useful property of the α_i is that a subgenerator can be "switched off" by putting the corresponding α_i to zero; the channel will then never be chosen. In particular, if $\alpha_5 = 0$, only eeγ events will be generated. If a kinematical configuration is known to be ruled out by the experimental cuts, the channel dominating in that configuration can be suppressed or switched off. This can be done provided that w is set equal to zero in the "unwanted" situations, so as to avoid the occurrence of huge w values. This leads to the last and nicest aspect; experimental cuts can simply and directly be applied by setting $w = 0$ if the events are outside the cuts.

The above discussion is of course also applicable to other processes than ee $\to$ eeγ. We shall now start to focus on Bhabha scattering. As mentioned, the following ingredients are needed for our Monte Carlo treatment:

(i) approximate cross sections f_i and the appropriate sets of phase-space variables ϕ_i in which to write them;

(ii) analytical expressions or numerical results for the integrals σ_i;

(iii) algorithms to obtain the phase space variables ϕ_i from random numbers equidistributed between $[0,1)$. We assume these latter to be given by some standard (pseudo-)random-number generator [10], and only need to find the appropriate mappings.

In the next few sections we shall discuss these points in detail.

4. The soft photon cross section

We start our discussion of the various channels in Bhabha scattering with the elastic scattering process (1.1). The calculation of the complete one-loop corrected formula for this channel, described in I, is very nontrivial; on the other hand, from the point of view of Monte Carlo event generation, this channel is the simplest. In particular, since it describes a two-body final state, there is, in the absence of transverse polarization, only one nontrivial kinematical variable to be generated. Also, the complete formula for $d\sigma/d\Omega$ presented in I is analytically very complicated; but numerically the result is a very smooth function, with no strong peaks other than the forward peak already present in the Born approximation. For these two reasons a simple approach can be used, which we shall now discuss. Let us define the following function of one variable

$$F_c(x) = \frac{d\sigma}{d\Omega}(\cos\theta = x), \tag{4.1}$$

where the right-hand side denotes the result of I. In terms of computer programming, $F_c(x)$ is a function subprogram containing all the formulae of I. In the present paper we consider this subprogram as a black box, with one input variable $x = \cos\theta$ (other variable quantities such as $\sqrt{s}$, m_Z, m_W etc. are assumed to be constants whose values are fixed throughout the Monte Carlo generation). We do not consider the detailed form of $F_c(x)$, other than to note that for x close to 1, F_c behaves roughly as $(1-x)^{-2}$, and that around the Z^0 resonance the comparatively isotropic s-channel distribution is strongly enhanced. The evaluation of $F_c(x)$ is speeded up by several orders of magnitude by the use of an interpolation scheme; we first evaluate $F_c(x)$ at 40 equidistant points in the interval from $\cos\theta_{\max}$ to cos(20°), and 20 equidistant points in the interval from cos(20°) to $\cos\theta_{\min}$. After this, the value of $F_c(x)$ is determined by a form of cubic spline interpolation. This means that the whole set of complicated diagrams only has to be evaluated 60 times, irrespective of the number of events to be generated in channel 5. Therefore, complicated functions and time-consuming operations in I are no problem. We have checked that the interpolation reproduces the exact value of F_c with an error of at most 0.01%; by taking more points this can of course be reduced still further.

We now turn to the determination of σ_s. The behaviour of $d\sigma_5/d\Omega$ with $\cos\theta$ motivates a change of variable from $c = \cos\theta$ to u, where

$$\frac{du}{dc} = \frac{1}{(1-c)^2} + a_Z,$$

$$a_Z = \frac{as^2}{\left(s - m_Z^2\right)^2 + m_Z^2\Gamma_Z^2}. \tag{4.2}$$

The constant a_Z incorporates the s-channel resonance, and the factor a can be used to tune the relative importance of the two channels; we found empirically that for

$a \sim 10^{-2}$ the Born-level cross section $(\mathrm{d}\sigma/\mathrm{d}\Omega)_{\mathrm{Born}}$ is approximated for all $\sqrt{s}$ by a constant times $\mathrm{d}u/\mathrm{d}c$ to within a factor of about 10 over the whole angular range, so we expect the approximation to the corrected cross section also to be reasonable. Integrating eq. (4.2) and solving for c we find

$$u = u(c) = a_Z c + 1/(1-c),$$

$$c = c(u) = \frac{1}{2a_Z}\left\{a_Z + u - \left[(a_Z - u)^2 + 4a_Z\right]^{1/2}\right\}, \tag{4.3}$$

so that the differential cross section can now be rewritten as

$$\mathrm{d}\sigma = F_u(u)\,\mathrm{d}u,$$

$$F_u(u) = 2\pi F_c(c(u))\left[a_Z + (1 - c(u))^{-2}\right]^{-1}. \tag{4.4}$$

The result of this exercise is that instead of the strongly peaked F_c we now have a much smoother F_u, from which we can obtain a numerical value for the integrated cross section using, e.g., the trapezoidal rule

$$\sigma_5 = \frac{u_N - u_1}{N-1}\left[\tfrac{1}{2}F_u(u_1) + \tfrac{1}{2}F_u(u_N) + \sum_{k=2}^{N-1} F_u(u_k)\right], \tag{4.5}$$

where the u_k are equidistant in the interval from

$$u_1 = u(\cos\theta_{\max}) \qquad \text{to} \qquad u_N = u(\cos\theta_{\min}):$$

$$u_k = u_1 + \frac{k-1}{N-1}(u_N - u_1). \tag{4.6}$$

Of course, much more accurate quadrature formulae are available instead of eq. (4.6). Since, however, we aim at an accuracy of, say, 10^{-4} (because the second-order corrections are unknown anyway), the simple rule (4.6), with an accuracy of order N^{-2}, is quite sufficient. For our purposes N is, say, 1000.

We now come to the generation of Monte Carlo events. This is done by a simple hit-and-miss technique: denoting by ρ or ρ_i a random number* equidistributed in $[0,1)$, we proceed as follows

$$u = u_1 + (u_N - u_1)\rho_1. \tag{4.7}$$

If $\rho_2 F^{\mathrm{est}} > F_u(u)$, try again. Here the estimator F^{est} is defined as

$$F^{\mathrm{est}} = (1+b)\max_{k=1,\ldots,N} F_u(u_k), \tag{4.8}$$

and is obtained as a by-product of the integration in eq. (4.6). The factor $(1 + b)$ in

* For a discussion of our random number generator, see sect. 7.

eq. (4.8) is introduced to ensure that $F_u(u) < F^{\text{est}}$ for all u values; that way the exact F_u distribution is generated. In practice, we use $b = 0.01$ which seems to be all right for $N = 1000$. Notice that with increasing b the expected speed of the algorithm (4.7) decreases as $(1+b)^{-1}$. Since the evaluation of F^u is so fast we can therefore, in principle, choose b much larger (of order 1, say) without slowing the event generation down appreciably. Once a value for u has been generated, the computation of $\cos\theta$ from eq. (4.3) and the construction of the four-momenta q_+^μ and q_-^μ is of course trivial; k^μ is taken to be zero in this case (see, however, the interesting results in ref. [12]). We were able to make the treatment of the virtual and soft photon corrections very fast, as a consequence of the essential one-dimensionality of the soft photon region. In the hard photon region, which we shall now discuss, another strategy will have to be employed.

We finish this section by pointing out that, since we know the exact value of the soft photon cross section, and the elastic events (1.1) will be generated with the correct angular distribution, the event weight from this channel is just a constant

$$w(\phi) = \frac{1}{\alpha_5}. \tag{4.9}$$

Here α_5 is the a priori weight assigned to the soft photon channel, as discussed in sect. 3.

5. Channels for the hard photon cross section

Because of both its multidimensionality and its peaked structure, the hard photon cross section discussed in sect. 2 calls for a slightly more sophisticated treatment than that of the soft photon. Upon studying the 16 Feynman graphs of fig. 1 it is clear that we can distinguish several groups which dominate the cross section in different parts of the phase space. These are the following.

Channel 1 (a, b) – *initial-state radiation in the photon s-channel.* These graphs give rise to the low-energy peak (c) of section 2, and dominate generally if $\sqrt{s} < m_Z$, especially if the photon is emitted at small angles.

Channel 2 (e, f, g, h) – *final-state radiation.* This is important if the photon is close to the outgoing e^+ or e^-, and dominates if $\sqrt{s} \sim m_Z$, at large angles of the e^+, e^-.

Channel 3 (c, d) – *initial-state radiation in the Z^0 s-channel.* This is similar to channel 1 except that it tends to yield e^+e^- pairs with mass $\sim m_Z$. For $\sqrt{s} \gtrsim m_Z$ it dominates at large angles.

Channel 4 (i, j, m, n) – *t-channel radiative scattering.* This dominates for all $\sqrt{s}$ at small scattering angles of the e^+ or e^-, and is described by QED only.

The remaining diagrams (k, l, o, p) and the interference between the various groups of diagrams are much less important, and are taken into account in the weights assigned to the Monte Carlo events, described in sect. 3. It is the distribu-

tion of these event weights, obtained in a Monte Carlo run, that ultimately justifies our choice of channels; however, that the above split-up is reasonable can be argued by simply looking at the various propagators.

We shall now proceed to derive the various approximants f_i. First of all, we remark that the mass effect factors W_m of eq. (2.7) will be incorporated in the event weight; so for the moment we may neglect m_e. For massless electrons, simple expressions are available [7] for the spin-summed/averaged squares of the various subsets of diagrams. Denoting by M_i the set of diagrams in channel i, we have

$$\overline{|M_1|^2} = \frac{e^6}{s'(p_+\cdot k)(p_-\cdot k)}[t^2+t'^2+u^2+u'^2], \tag{5.1}$$

$$\overline{|M_2|^2} = \frac{e^2}{s(q_+\cdot k)(q_-\cdot k)} \times\left[(t^2+t'^2+u^2+u'^2)\left(e^4+2v^2\frac{s(s-m_Z^2)}{B(s)}+(v^2+a^2)^2\frac{s^2}{B(s)}\right)\right.$$
$$\left.+(u^2+u'^2-t^2-t'^2)\left(2a^2\frac{s(s-m_Z^2)}{B(s)}+4v^2a^2\frac{s^2}{B(s)}\right)\right], \tag{5.2}$$

$$\overline{|M_3|^2} = \frac{e^2s'}{B(s')(p_+\cdot k)(p_-\cdot k)}\left[(v^2+a^2)^2(t^2+t'^2+u^2+u'^2)\right.$$
$$\left.+4v^2a^2(u^2+u'^2-t^2-t'^2)\right], \tag{5.3}$$

$$\overline{|M_4|^2} = \frac{e^6}{tt'}(s^2+s'^2+u^2+u'^2) \times\left[\frac{s}{(p_+\cdot k)(p_-\cdot k)}+\frac{s'}{(q_+\cdot k)(q_-\cdot k)}-\frac{t}{(p_+\cdot k)(q_+\cdot k)}\right.$$
$$\left.-\frac{t'}{(p_-\cdot k)(q_-\cdot k)}+\frac{u}{(p_+\cdot k)(q_-\cdot k)}+\frac{u'}{(p_-\cdot k)(q_+\cdot k)}\right]. \tag{5.4}$$

Here, $B(s)$ stands for the Z^0 resonance shape

$$B(s) = (s-m_Z^2)^2+m_Z^2\Gamma_Z^2. \tag{5.5}$$

We proceed to modify eqs. (5.1)–(5.4) in order to arrive at the approximants. To this end we first note that $t^2+t'^2+u^2+u'^2 \leqslant s^2+s'^2$ in the whole phase space.

Also, in eq. (5.4) the four terms in the last factor (with s, s', u and u'), which describe the interference between radiation from the electron line and positron line, can be expected to be small whenever channel 4 is important (i.e. e^+ and/or e^- at small angles). Applying this we arrive at the following approximants

$$A_1 = \frac{e^6}{s'(p_+\cdot k)(p_-\cdot k)}(s^2+s'^2), \tag{5.6}$$

$$A_2 = \frac{e^2}{(q_+\cdot k)(q_-\cdot k)}D(s)(s^2+s'^2), \tag{5.7}$$

$$D(s) = \frac{e^4}{s} + 2(v^2+a^2)\frac{s-m_Z^2}{B(s)} + (v^4+6v^2a^2+a^4)\frac{s}{B(s)},$$

$$A_3 = \frac{e^2(v^4+6v^2a^2+a^4)(s^2+s'^2)s'}{B(s')(p_+\cdot k)(p_-\cdot k)}, \tag{5.8}$$

$$A_4 = e^6(s^2+s'^2)\left(\frac{-1}{t'(p_+\cdot k)(q_+\cdot k)} + \frac{-1}{t(p_-\cdot k)(q_-\cdot k)}\right). \tag{5.9}$$

According to the prescription given in sect. 3, whenever a Monte Carlo event is generated in channels 1, 2, 3 or 4 its weight will be computed as

$$w = \frac{\overline{|M|^2}}{\alpha_1 A_1 + \alpha_2 A_2 + \alpha_3 A_3 + \alpha_4 A_4}. \tag{5.10}$$

The next step is the computation of the cross sections σ_i corresponding to the various channels. This we shall do in sect. 6.

6. Boundaries and integrals

Before we can calculate the integrals σ_i ($i = 1,2,3,4$) of the approximants A_i we have to choose those phase-space elements $d\Phi$ that are most appropriate for each channel. These are: eq. (2.9a) for A_2, eq. (2.9b) for A_4, and eq. (2.9c) for both A_1 and A_3. Also, we will have to take the nonzero value of the electron mass m_e into account in the products $p_\pm\cdot k$ and $q_\pm\cdot k$, since we are going to integrate over the collinear peaks.

The multidifferential cross section for channel 1 can be written as

$$d^5\sigma_1 = \frac{\alpha^3}{4\pi^2 s}\frac{1+(1-k)^2}{k(1-k)}\frac{1}{(p_+\cdot k)(p_-\cdot k)}\,dk\,d\Omega_e\,dz_\gamma\,d\phi_\gamma,$$

$$p_\pm\cdot k = kE_b^2(e\mp z_\gamma)+O(m^4), \qquad e=1+\tfrac{1}{2}m^2, \qquad m=m_e/E_b, \tag{6.1}$$

where k is the photon energy k^0 normalized to the beam energy E_b, and z_γ is the cosine of the angle between $\boldsymbol{k}$ and $\boldsymbol{p}_+$ and ϕ_γ the azimuthal angle of $\boldsymbol{k}$ around $\boldsymbol{p}_+$. The only nontrivial integrals are those over z_γ and k. We obtain

$$\sigma_1 = \frac{2\alpha^3}{s}\ln\frac{s}{m_e^2}\left[H_1(k_{max})-H_1(k_0)\right],$$

$$H_1(k) = 2\ln k - \ln(1-k) - k. \tag{6.2}$$

Here, k_0 is $\Delta E/E_b$, i.e. the minimum value of k, and k_{max} is the maximum value of k that we want to allow in the Monte Carlo event sample. A difficulty arises if we do not want to impose an upper bound on k: $H_1(k)$ diverges as $k\to 1$. In reality, the endpoint of the photon spectrum behaves as [13]

$$\lim_{k\to 1}\frac{d\sigma_1}{dk} \propto \frac{1}{1-k}\left(1+\frac{2m_e^2}{s'}\right)\left(1-\frac{m_e^2}{s'}\right)^{1/2}, \tag{6.3}$$

rather than as $(1-k)^{-1}$, for finite m_e. We solve this problem by defining an effective supremum k_{sup} such that σ_1 with $k_{max}=k_{sup}$ has precisely the correct area under the photon spectrum curve. This value turns out to be

$$k_{sup} = 1-\frac{m_e^2}{s}\exp\left(\tfrac{5}{3}\right). \tag{6.4}$$

Using this value, we ensure that the total number of events eeγ with very-low-invariant-mass ee pairs will be correct. The angular distribution of these pairs *in their centre-of-mass frame* will not be correct; but for pairs of such extremely low mass this is unimportant.

Channel 2 is most easily treated by noticing that the expression (5.7) is symmetric in $q_\pm^\mu \leftrightarrow q_\mp^\mu$. Provided that in the Monte Carlo generation of events we apply this symmetry, we may write

$$d^5\sigma_2 = \frac{\alpha}{64\pi^4}D(s)\frac{1+(1-k)^2}{k(1-x+\delta)}\,dx\,dk\,d\Omega\,d\phi_\gamma,$$

$$\delta = m_e^2 k/s', \tag{6.5}$$

where x is the positron energy q_+^0 in units of E_b. A derivation of the expression $2E_b^2(1-x+\delta)$ for $q_-\cdot k$ can, for instance, be found in ref. [13]. Integrating over $d\Omega$ and $d\phi_\gamma$, and over x from the kinematical limits $1-k$ up to 1, we find

$$\frac{d\sigma}{dk} = \frac{\alpha}{8\pi^2} D(s) \frac{1+(1-k)^2}{k} \ln\left(\frac{s(1-k)}{m_e^2}\right), \tag{6.6}$$

and for the total cross section between $k = k_0$ and $k = k_{max}$

$$\sigma_2 = \frac{\alpha}{8\pi^2} D(s)\left[H_2(k_{max}) - H_2(k_0)\right],$$

$$H_2(k) = \left[2\ln k - 2k + \tfrac{1}{2}k^2\right]\ln\frac{s}{m_e^2} - 2\,\mathrm{Li}_2(k)$$

$$+ \tfrac{1}{2}(3-k)(1-k)\ln(1-k) - \tfrac{1}{4}(5-k)(1-k), \tag{6.7}$$

where Li_2 denotes the dilogarithm function. It should be noted that $H_2(k)$ remains finite as $k \to 1$; for consistency reasons, however, we shall always use, at most, k_{sup}, as defined in eq. (6.4), in $H(k)$ as well.

Channel 3 differs from channel 1 only in its overall factor and photon spectrum. We have:

$$d^5\sigma_3 = \frac{\alpha(v^4+6v^2a^2+a^4)}{64\pi^4 s} \frac{(1-k)\left[1+(1-k)^2\right]}{\left[(k-\xi)^2+\gamma^2\right]k} \frac{1}{e^2 - z_\gamma^2}\, dk\, d\Omega\, d\Omega_\gamma,$$

$$\xi = 1-\mu, \qquad \mu = m_Z^2/s, \qquad \gamma = m_Z\Gamma_Z/s, \tag{6.8}$$

which can be integrated over $d\Omega\, d\Omega_\gamma$ to give the photon spectrum

$$d\sigma_3/dk = \frac{\alpha(v^4+6v^2a^2+a^4)}{8\pi^2 s} \ln\left(\frac{s}{m_e^2}\right) \frac{(1-k)(2-2k+k^2)}{k\left[(k-\xi)^2+\gamma^2\right]}, \tag{6.9}$$

and the total cross section

$$\sigma_3 = \frac{\alpha(v^4+6v^2a^2+a^4)}{8\pi^2 s} \ln\left(\frac{s}{m_e^2}\right)\left[H_3(k_{max}) - H_3(k_0)\right],$$

$$H_3(k) = h_1 \ln k + \tfrac{1}{2}h_2 \ln\left[(k-\xi)^2+\gamma^2\right] + h_3 \arctan\left(\frac{k-\xi}{\gamma}\right) - k,$$

$$h_1 = 2\left(\xi^2+\gamma^2\right)^{-1},$$

$$h_2 = 3 - 2\xi - h_1,$$

$$h_3 = \left[\xi h_1 - 4 + 3\xi - \xi^2 + \gamma^2\right]/\gamma. \tag{6.10}$$

Like H_2, H_3 is regular for $k \to 1$. Due to the presence of the two mass scales s and m_Z^2 in the spectrum, its form is quite complicated; for a discussion, see for instance, refs. [14,15].

Our treatment of channel 4 is essentially the same as was given for pure-QED Bhabha scattering in ref. [15]. Again, we employ the symmetry of eq. (5.9) under the interchange of electrons and positrons to retain only the term with $[t(p_- \cdot k)(q_- \cdot k)]^{-1}$, and find

$$d^5\sigma_4 = \frac{2\alpha^3}{\pi^2 s} \frac{1+(1-k)^2}{k} \frac{1}{1-c} \frac{1}{e+z} \frac{1}{e+c_\gamma} dk\, d\Omega\, d\Omega_\gamma, \tag{6.11}$$

where z is the cosine of angle between $\boldsymbol{k}$ and $\boldsymbol{p}_+$, and c_γ that of the angle between $\boldsymbol{k}$ and $\boldsymbol{q}_+$. In this channel the most complicated integral is that over Ω_γ rather than over k. It is most simply and elegantly solved by applying the Feynman integral parametrization, which introduces one additional dimension into the integral. This is described in detail in ref. [15]. We end up with

$$d^2\sigma_4 = \frac{16\alpha^3}{s} \frac{1+(1-k)^2}{k} dk \frac{\ln(2(1-c)/m^2)}{(1-c)^2} dc, \tag{6.12}$$

so that

$$\sigma_4 = \frac{16\alpha^3}{s} [H_4(k_{\max}) - H_4(k_0)][F(\cos\theta_{\min}) - F(\cos\theta_{\max})],$$

$$H_4(k) = 2\ln k - 2k + \tfrac{1}{2}k^2,$$

$$F(c) = [1 + \ln(2(1-c)/m^2)]/(1-c). \tag{6.13}$$

This integral forces us to include also the minimum and maximum allowed scattering angles $\theta_{\min,\max}$ as a priori cuts on the phase space, which leads to the following observation. In all channels, k appears as one of the integration variables, and consequently a priori cuts on k are easy; no generated Monte Carlo event will have $k < k^0$ or $k > k_{\max}$. However, c appears as an integration variable only in σ_4. Therefore, some events generated in channels 1, 2 or 3 will have $c > \cos\theta_{\min}$ or $c < \cos\theta_{\max}$. Moreover, since in channel 4 we are only able to restrict the direction of $\boldsymbol{q}_+$, not of $\boldsymbol{q}_-$, also $\boldsymbol{q}_-$ will sometimes fall outside of the admissible range. Since no peak of the cross section is associated to such events (remember that the peak for $t' \to 0$ is obtained afterwards by symmetrization) the number of these events, which of course have to be rejected, is modest.

At this point, several of the Monte Carlo ingredients have been obtained. We have the approximants A_i, and the total cross sections σ_i corresponding to them.

Also, the exact matrix element can be calculated as soon as the momenta q_+^μ, q_-^μ and k^μ of a Monte Carlo event are specified. The last necessary part, the algorithms to obtain these values, is discussed in sect. 7.

7. Generation algorithms

We shall now discuss the methods used to generate Monte Carlo events, that is, a set of phase-space variables appropriate to the particular channel (1–4) chosen, distributed randomly with probability densities proportional to one of eqs. (5.6)–(5.9). An excellent review of the methods available to generate random variables with a specified distribution is given in ref. [16]. We assume the existence of a source of satisfactorily random real numbers equidistributed between $[0,1)$; in practice we use the CERNLIB routine RN32 given in ref. [10]. These numbers are subsequently transformed by mappings and rejection procedures so as to ensure the correct distribution. The above random-number generator can, of course, be replaced by any other generator in which the user has confidence, without changing anything but the statistical fluctuations in our results. As in sect. 4, we shall denote the above random numbers by $\rho_{(i)}$. We now list the various algorithms; for proofs that these do give the correct distributions we refer the reader to refs. [11] and [16].

7.1. CHANNEL 1

The photon spectrum is generated by a combination of mapping (to obtain the two peaks for small and large values for k) and rejection (refining the distribution so as to have the correct factor $2-2k+k^2$)

$$k=\left[1+\exp\left(-\ln\frac{k_0}{1-k_0}-\rho_1\ln\frac{k_{\max}(1-k_0)}{k_0(1-k_{\max})}\right)\right]^{-1},$$

$$w_1=\left(1+(1-k)^2\right)\Big/\left(1+(1-k_0)^2\right), \tag{7.1}$$

$$\text{if } w_1<\rho_2, \qquad \text{try again}.$$

The boundaries k_0 and $k_{\max}$ on the k-spectrum have been defined in sect. 6. The angular variable z_γ requires only a simple mapping. Using $\varepsilon=m_e^2/2E^2$, we have

$$v=\exp\left(\ln\varepsilon+\rho_3\ln\frac{2+\varepsilon}{\varepsilon}\right)-\varepsilon,$$

$$z_\gamma=1-v, \qquad s_\gamma=(v(2-v))^{1/2}, \tag{7.2}$$

$$\text{if } \rho_4>\tfrac{1}{2}, \qquad \text{replace } z_\gamma \text{ by } -z_\gamma.$$

It should be noted that due to the smallness of ε (about 5×10^{-11} at LEP I energies), the typical value attained by $|z_\gamma|$ is very close to 1. This would make the computation of $s_\gamma = \sin\sphericalangle(\boldsymbol{k}, \boldsymbol{p}_+) = \sqrt{1 - z_\gamma^2}$ numerically unstable. By generating not z_γ but $v = 1 - |z_\gamma|$, which is typically small (median about $\sqrt{2}\,\varepsilon$), the accuracy of s_γ is improved by quite a few digits. The other variables are obtained trivially

$$\phi_\gamma = 2\pi\rho_5\,, \qquad \phi_R = 2\pi\rho_6\,, \qquad \cos\theta_R = 2\rho_7 - 1\,, \tag{7.3}$$

where ϕ_R and θ_R are the two Euler angles of the outgoing e^+ in the e^+e^- c.m.s.; since these angles are trivially distributed their orientation is irrelevant, and we take $\theta_R = 0$ to correspond to the positive z-axis. From the five variables k, z_γ, ϕ_γ, $\cos\theta_R$ and ϕ_R the four-momenta q_+^μ, q_-^μ and k^μ are easily constructed, and can be used to compute the matrix element. However, some care is necessary in the computation of $p_+ \cdot k$, $p_- \cdot k$ and W_m since significant cancellations are to be expected. We tackle this problem in two ways. Firstly, the factors $|s(p, k)|^2/(2p \cdot k)$ in W_m in eq. (2.7) were necessitated because $s(p, k)$ and $p \cdot k$ do not behave in precisely the same way in the collinear situation $\boldsymbol{k} \parallel \boldsymbol{p}$. We are, however, not interested in the squared matrix element (2.1) itself but only in the weight function defined in eq. (3.3). Therefore, if we replace the denominators $(p_\pm \cdot k)$ and $(q_\pm \cdot k)$ in eqs. (5.6)–(5.9) by $\frac{1}{2}|s(p_\pm, k)|^2$ and $\frac{1}{2}|s(q_\pm, k)|^2$ *in the computation of the weight*, and keep the correct expressions in the calculation of σ_{1-4} in sect. 6, we can disregard the incorrect behaviour at the peaks; *the weight* will be computed correctly. Moreover, at most only one of the four remaining factors in eq. (2.7) can differ appreciably from 1 for any event. The consequence of all this is, that for events generator in channel 1, we may compute W_m as

$$W_m = 1 - \frac{2\varepsilon}{\varepsilon + v} \cdot \frac{(1-k)}{1 + (1-k)^2}\,. \tag{7.4}$$

This form for W_m is independent of the sign flip of z_γ in eq. (7.2), and gives the correct suppression due to the mass effect up to $O(m_e^2/s)$.

7.2. CHANNEL 2

Again the photon spectrum is obtained by combining mapping and rejection

$$k = k_0(k_{\max}/k_0)^{\rho_1}\,,$$

$$w_2 = \left[\left(1 + (1-k)^2\right)\ln\frac{s(1-k)}{m_e^2}\right] \Bigg/ \left[\left(1 + (1-k_0)^2\right)\ln\frac{s(1-k_0)}{m_e^2}\right], \tag{7.5}$$

if $w_2 < \rho_2$, try again.

The variable x is given by a k-dependent mapping

$$\delta = m_e^2 k/s(1-k),$$

$$v_x = \exp\left[\ln\delta + \rho_3 \ln\frac{k+\delta}{\delta}\right] - \delta,$$

$$x = E_b(1-v_x). \tag{7.6}$$

The angular variables Ω_+ and ϕ_a are again trivially generated as in eq. (7.3). As in channel 1, the cosine c_γ and sine s_γ of the angle between $\boldsymbol{q}_+$ and $\boldsymbol{k}$, which tends to be close to 180°, have to be computed carefully, using

$$v_\gamma = \frac{2v_x(1-k)}{k(1-v_x)}, \qquad c_\gamma = v_\gamma - 1, \qquad s_\gamma = \left(v_\gamma(2-v_\gamma)\right)^{1/2}. \tag{7.7}$$

After the four-momenta have been constructed, q_+^μ and q_-^μ have to be interchanged in one half of the events, as described in sect. 6. Finally, in this channel the mass effect is incorporated as

$$W_m = 1 - \frac{\varepsilon}{v_x+\delta}\cdot\frac{k}{1+(1-k)^2}. \tag{7.8}$$

Again, this definition is independent of the interchange of q_+^μ and q_-^μ.

7.3. CHANNEL 3

As stated before, the shape of the photon spectrum in the Z^0-exchange s-channel is complicated by the occurrence of different mass scales. No simple combination of mapping and rejection is known to us which would be efficient for all possible combinations of s and M_Z. Instead we rely on a purely numerical method, which was introduced and explained in detail in ref. [17]. We construct a histogram of the photon spectrum with, say, 1000 bins, such that all bins have the same area to a very good approximation. The total area under the histogram can be compared to the purely analytical result (6.10) to provide a check. Subsequently, a k value is generated by choosing a bin at random, and generating a k value uniformly distributed in the bin. This procedure yields a distribution equal to the desired one to a very good approximation. In particular the soft photon and Z^0 resonance peak are accurately described because the bins are quite narrow in that region. For completeness we summarize this algorithm in appendix B.

The remaining algorithms for this channel are precisely the same as for channel 1.

7.4. CHANNEL 4

As stated before, this channel is just QED Bhabha scattering, and the discussion of ref. [15] can be carried over without modification; only the photon spectrum contains an additional factor $1+(1-k)^2$ in the present case (in ref. [15] this factor was neglected in order to make the weights better behaved for $k \to 1$; since in this paper we explicitly include channel 1 this is not necessary here). Again, the photon spectrum is given by mapping and rejection

$$\begin{aligned} &k = k_0 (k_{\max}/k_0)^{\rho_1}, \\ &w_4 = (1+(1-k)^2)\Big/(1+(1-k_0)^2), \\ &\text{if } w_4 < \rho_2, \qquad \text{try again}. \end{aligned} \tag{7.9}$$

The cosine c of the angle between $\boldsymbol{q}_+$ and $\boldsymbol{p}_+$ is obtained via a similar rule

$$\begin{aligned} &c = 1 - \left[\rho_3 (1-\cos\theta_{\min})^{-1} + (1-\rho_3)(1-\cos\theta_{\max})^{-1}\right]^{-1}, \\ &w_c = \ln\left(\frac{1-c}{\varepsilon}\right)\Big/\ln\left(\frac{1-\cos\theta_{\max}}{\varepsilon}\right), \\ &\text{if } w_c < \rho_4, \qquad \text{try again}, \end{aligned} \tag{7.10}$$

while the corresponding azimuthal angle ϕ is again trivial. The algorithm for the photon direction is more complicated, since its distribution peaks for both $\boldsymbol{k} \parallel \boldsymbol{p}_-$ and $\boldsymbol{k} \parallel \boldsymbol{q}_-$ (cf. eq. (6.11)). As explained in ref. [15] we solve this by the Feynman trick, by which we write the distribution of the photon solid angle as a superposition of distributions with a more peaked behaviour, each distribution oriented with respect to a linear combination (parametrized by the Feynman variable u) of the directions of $\boldsymbol{p}_-$ and $\boldsymbol{q}_-$ (see eq. (4.2) of [15]). A Feynman variable is now picked according to the following prescription

$$\begin{aligned} &u_0 = \varepsilon/(1-c), \qquad u_1 = 1+u_0, \\ &u = \exp(\ln u_0 + \rho_5 \ln(u_1/u_0)) - u_0, \\ &\text{if } \rho_6 > \tfrac{1}{2}, \text{ replace } u \text{ by } 1-u. \end{aligned} \tag{7.11}$$

The choice of u determines a particular linear combination of the directions $\boldsymbol{p}_-/|\boldsymbol{p}_-|$ and $\boldsymbol{q}_-/|\boldsymbol{q}_-|$. For the moment we assume this direction to be the positive z-axis. The recipe for c', the cosine of the angle between $\boldsymbol{k}$ and this axis, and for $s_{c'}$

and $\phi_{c'}$, the corresponding sine and azimuthal angle, is then

$$
\begin{aligned}
&e_2 = 2(1-c)(u_1-u)(u+u_0),\\
&e_u = (1+2\varepsilon-e_2)^{1/2},\\
&v' = 2e_2(1-\rho_7)\big[e_2+2\rho_7 e_u(1+2\varepsilon+e_u)\big]^{-1},\\
&c' = 1-v', \qquad s_{c'} = \big(v'(2-v')\big)^{1/2},\\
&\phi_{c'} = 2\pi\rho_8 .
\end{aligned}
\tag{7.12}
$$

The direction $\boldsymbol{e}_k$ of $\boldsymbol{k}$ in the lab frame is, finally, obtained by rotating the positive z-axis to the actual direction specified by the Feynman variable u

$$
\begin{aligned}
&e_k^x = \Big[s_{c'}\cos\phi_{c'}(u-1-uc) - uc'(1-c^2)^{1/2}\Big]\Big/e_u,\\
&e_k^y = s_{c'}\sin\phi_{c'},\\
&e_k^z = \Big[us_{c'}\cos\phi_{c'}(1-c^2)^{1/2} + (u-1-uc)c'\Big]\Big/e_u .
\end{aligned}
\tag{7.13}
$$

The four-momenta can now be constructed without more ado. Notice that, since $c = \cos\sphericalangle(\boldsymbol{p}_+, \boldsymbol{q})$ was restricted to be within the range between $\cos\theta_{\max}$ and $\cos\theta_{\min}$, the symmetrization $q_+^0 \leftrightarrow q_-^0$, $\boldsymbol{q}_+ \leftrightarrow -\boldsymbol{q}_-$ and $\boldsymbol{k} \to -\boldsymbol{k}$ (which we have to apply in $\frac{1}{2}$ of the cases) forces us to reject an event that has $\cos < (\boldsymbol{p}_-, \boldsymbol{q}_-)$ outside this range. Fortunately, the number of these events is small, as discussed in sect. 6. The derivation of a numerically stable representation for this case is not trivial, again because of the variable distance between the two peaks in the direction of $\boldsymbol{k}$. We find

$$
\begin{aligned}
&\xi = u\Big((1-c^2)^{1/2}s_{c'}\cos\phi_{c'} + (1-c)c'\Big) + v',\\
&v = \big(\xi + (2\varepsilon - e_2)/(1+e_u)\big)/e_u,\\
&W_m = 1 - \frac{\varepsilon}{\varepsilon+v}\cdot\frac{2(1-k)}{1+(1-k)^2} .
\end{aligned}
\tag{7.14}
$$

Again, this is independent of the replacement $u \to 1-u$ in eq. (7.11). This finishes our description of the generation algorithms. When an event has been generated, it must be checked whether it is within the allowed phase space; both $\boldsymbol{q}_+$ and $\boldsymbol{q}_-$ must have polar angles between $\theta_{\min}$ and $\theta_{\max}$. If the event fails this check the weight has to be put to zero (in practice the program then tries again, while storing the

zero-weight result in a bookkeeping device). If the event is admissible, its weight is calculated, keeping in mind the remarks made in connection with the computation of W_m. The event and its weight are then output. Optionally, there is an internal additional rejection to obtain unweighted events.

8. Results

After having discussed, in the previous sections, how the Monte Carlo approach to radiative corrections, together with the particulars of Bhabha scattering, led to the algorithms which we have described, it is now time for a review of the physics results, obtained with the Monte Carlo program. Throughout the discussion we have used the following parameter choices

$$m_Z = 93 \text{ GeV}, \qquad m_{\text{top}} = 40 \text{ GeV}, \qquad m_{\text{Higgs}} = 100 \text{ GeV}, \tag{8.1}$$

which lead to a value of 2.464 GeV for Γ_Z, 82 GeV for m_W, and hence 0.2227 for $\sin^2\theta_w$. Our results do not, however, change qualitatively for reasonable changes in the parameters (8.1).

We start with some remarks on the choice of ΔE, the cut-off between the hard and soft photon regions. As discussed in sect. 4, Monte Carlo events from channel 5 (the soft photon and virtual corrections) have a photon with an energy which is strictly zero. This is, of course, an approximation to the real situation in which an unlimited number of arbitrarily soft photons is emitted [18]. Recently, algorithms have been developed to deal with these photons [12]; however, the kinematics of the remainder of the event, and in particular its recoil (which gives rise to e.g. e^+e^- pairs with extremely small but nonzero acollinearity) is not yet understood very well. We therefore stick to putting k_0 to zero in the soft photon region. This, however, forces us to choose $\Delta E/E_b$ as small as possible. A logical lower limit on ΔE is that value that makes $d\sigma_{ee}/d\Omega$ (as defined in sect. 3) vanish, i.e. the sum of virtual and soft-photon corrections are exactly 100% (of course, the contributions from hard bremsstrahlung, with $k_0 > \Delta E$ are always positive). This approach has been taken successfully in ref. [16]. In the present case, however, the corrections depend on θ; generally, they decrease with increasing θ. We therefore determined θ_x, defined to be that value of θ for which $d\sigma_{ee}/d\Omega$ becomes zero, for the energy range of interest, for various values of $\Delta E/E_b$. The result is given in fig. 2. For $\Delta E/E = 10^{-2}$, $\theta_x(E_b)$ is quite well-behaved. In particular, at the resonance ($E_b = 46.5 \text{ GeV} = m_Z/2$)$\theta_x$ is essentially 180°, so that $d\sigma_{ee}/d\Omega$ is positive for all scattering angles. Outside this region the cross section is well-defined up to scattering angles of at least 170°. Since Bhabha scattering favours small angles so much, this is quite acceptable. A drastically different situation arises if we decrease the value of $\Delta E/E_b$ to 5×10^{-3}. Especially at the resonance, θ_x drops to a spectacular 122.1 degrees. This means that, for this value of $\Delta E/E$, a Monte Carlo study of Z^0

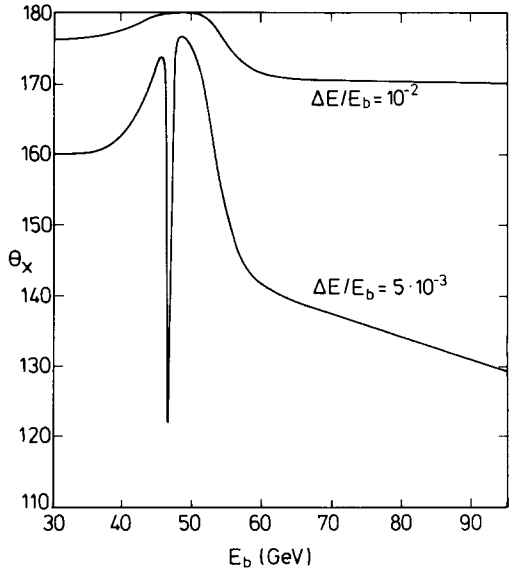

Fig. 2. Boundaries of the area of positivity of $d\sigma_{ee}/d\Omega$ as a function of beam energy, for different values of the soft-photon cutoff $\Delta E/E_b$.

production at the resonance is meaningless for all those events that have an angle between its incoming and outgoing electrons larger than 122 degrees! This is clearly unacceptable. At higher energies the situation is not very much better. The transition from the well-behaved to the ill-behaved cross section is sketched in table 1, where we give θ_x at the fixed resonance beam energy of 46.5 GeV, for varying $\Delta E/E_b$. The value of θ_x is seen to drop quite suddenly when $\Delta E/E_b$ decreases from 0.7% to 0.5% (for values of $\Delta E/E_b$ larger than 1%, θ_x remains at 180 degrees). We can draw two conclusions.

(1) A lower limit on $\Delta E/E_b$ is naturally given to be about 0.7% (in practice we have always used 1%).

(2) Any experimental setup which is sensitive to values of $\Delta E/E_b$ smaller than 1% (for instance, an angular resolution which makes an acollinearity determination

TABLE 1

Position of the zero in $d\sigma_{ee}/d\Omega$ at resonance ($\sqrt{s} = m_Z$) as a function of the soft-photon cutoff $\Delta E/E_b$

$\Delta E/E_b$ (%)	θ_x (deg)	$\Delta E/E_b$ (%)	θ_x (deg)
1.0	179.97	0.5	122.1
0.9	179.9	0.4	71.7
0.8	179.2	0.3	46.8
0.7	176.4	0.2	31.5
0.6	164.4	0.1	12.4

down to 0.5 degrees possible) will necessitate the inclusion of higher order corrections to make a study of resonant Z^0 production meaningful. Note that, here, the issue is not so much whether the Standard model can be tested to one-loop accuracy, but whether it can be tested at all.

The second point of interest is the total radiative correction. In contrast to the case of muon pair production, this concept has to be defined carefully here, due to the forward singularities. In the Born approximation, both e^+ and e^- will always be

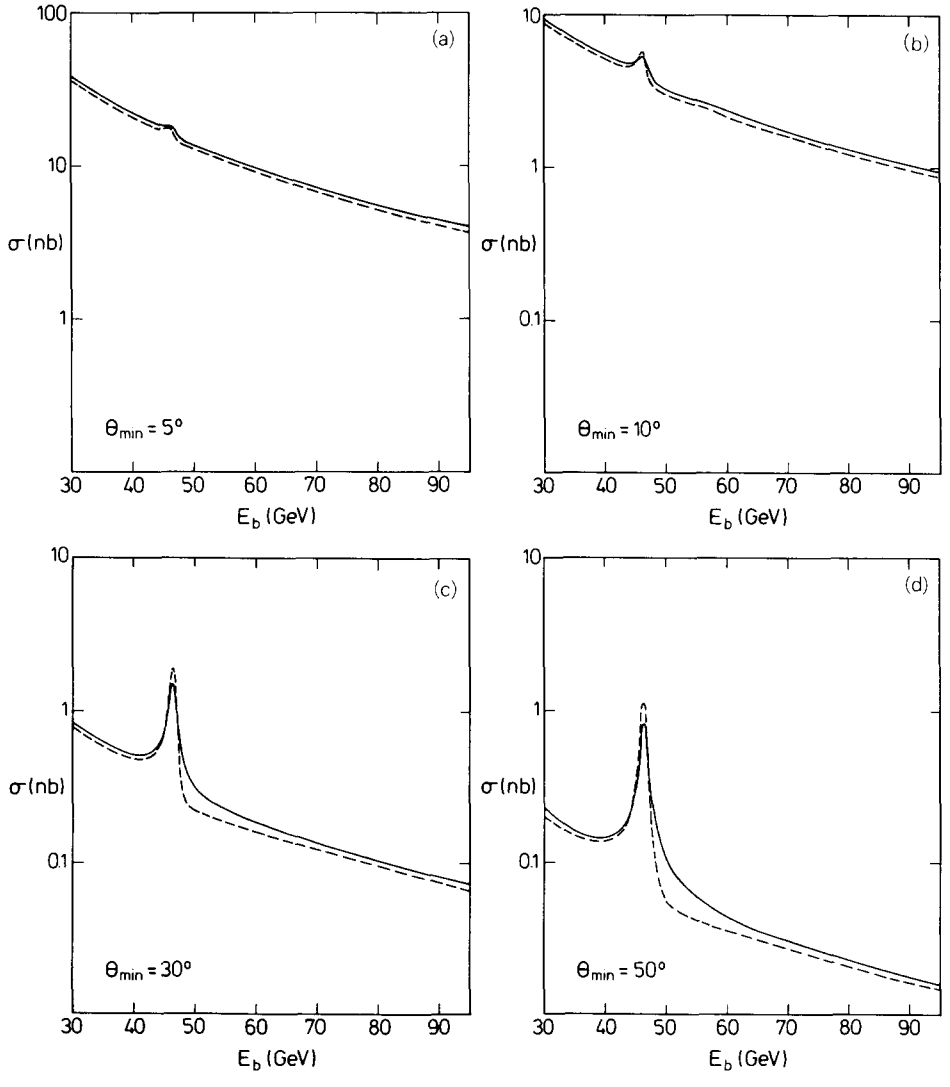

Figs. 3(a)–(d). Born cross section and total radiative correction as a function of beam energy, for various angular ranges. Dashed line: lowest order, solid line: corrected result.

restricted in the same angular range, because the events are elastic. We therefore define the total correction for a given angular range to be given by the total cross section for all events that have the scattering angles of the e^+ and e^- restricted between θ_{min} and θ_{max}, but with no additional cuts. We always take $\theta_{max} = 180° - \theta_{min}$, and studied four cases in detail: $\theta_{min} = 5°$, 10°, 30° and 50°. At $\theta_{min} = 5°$ the cross section is dominated by the t-channel photon graphs, while at $\theta_{min} = 50°$ the situation can be expected to look quite a bit like muon pair production. The two other cases are intermediate; $\theta_{min} = 30°$ is typical for experiments in a "central detector".

We have made runs of the MC program at various energies, for the four angular ranges specified above. Due to the forward peak, it is not practical to obtain the three smaller angular ranges by making cuts in the sample with $\theta_{min} = 5°$; hardly any events are left that way. Instead, separate runs are advisable. In each case we generated 10^4 weighted events (each run typically takes about 20 minutes on an IBM PC/AT). In figs. 3a to 3d we plot both the Born-term cross section and the cross section with the total correction discussed above. The Born cross section is obtained analytically, using the formula given in appendix C. A few qualitative features are evident. Firstly, at small θ_{min} the Z^0 "peak" is nearly invisible. Only at $\theta_{min} = 30$ is something like the muon-pair resonance evident. Furthermore, at the resonance the correction is actually *positive* for small θ. Being about 5%, this correction gives no indication of a necessity of higher order corrections in the photon exchange channel. Finally, the high radiative tail ($\sim 100\%$) of the resonance of higher energies which is familiar from the muon case is not evident for $\theta_{min} = 30°$ and $\theta_{min} = 50°$. This can be understood easily; the radiative tail originates from events in channel 3, where a hard photon is typically emitted close to the beam, with the fermion pair recoiling in the other direction. Such configurations tend to be rejected by the angular cuts on both the e^+ and e^-.

Of course, the total correction is not what is usually measured, which brings us to the topic of canonical cuts. In ref. [5] the application was advocated of *canonical cuts*, i.e. simple and well-defined cuts which reduce (if possible) the radiative corrections and, since they would be applied at least once by the relevant experiments, would allow for unambiguous comparison between the results of different experiments. For e^+e^- as well as $\mu^+\mu^-$ it seems that the best canonical cuts are the following set:

(1) the energies of the e^+ and e^- must be larger than some threshold value E_{th};

(2) the angle between the e^+ and e^- directions must be larger than $180° - \zeta$; ζ is called the acollinearity cut.

We apply $E_{th} = \frac{1}{2}E_b$ and $\zeta = 10$ degrees and of course the angular cuts discussed before. The effect of this choice of E_{th} is marginal, the acollinearity cut being much tighter; a motivation for the choice of ζ will be given later on.

In a figs. 4a–4d we present close-ups of the resonance region for the four values of θ_{min}. We draw both the Born cross section (dashed line), the fully corrected one

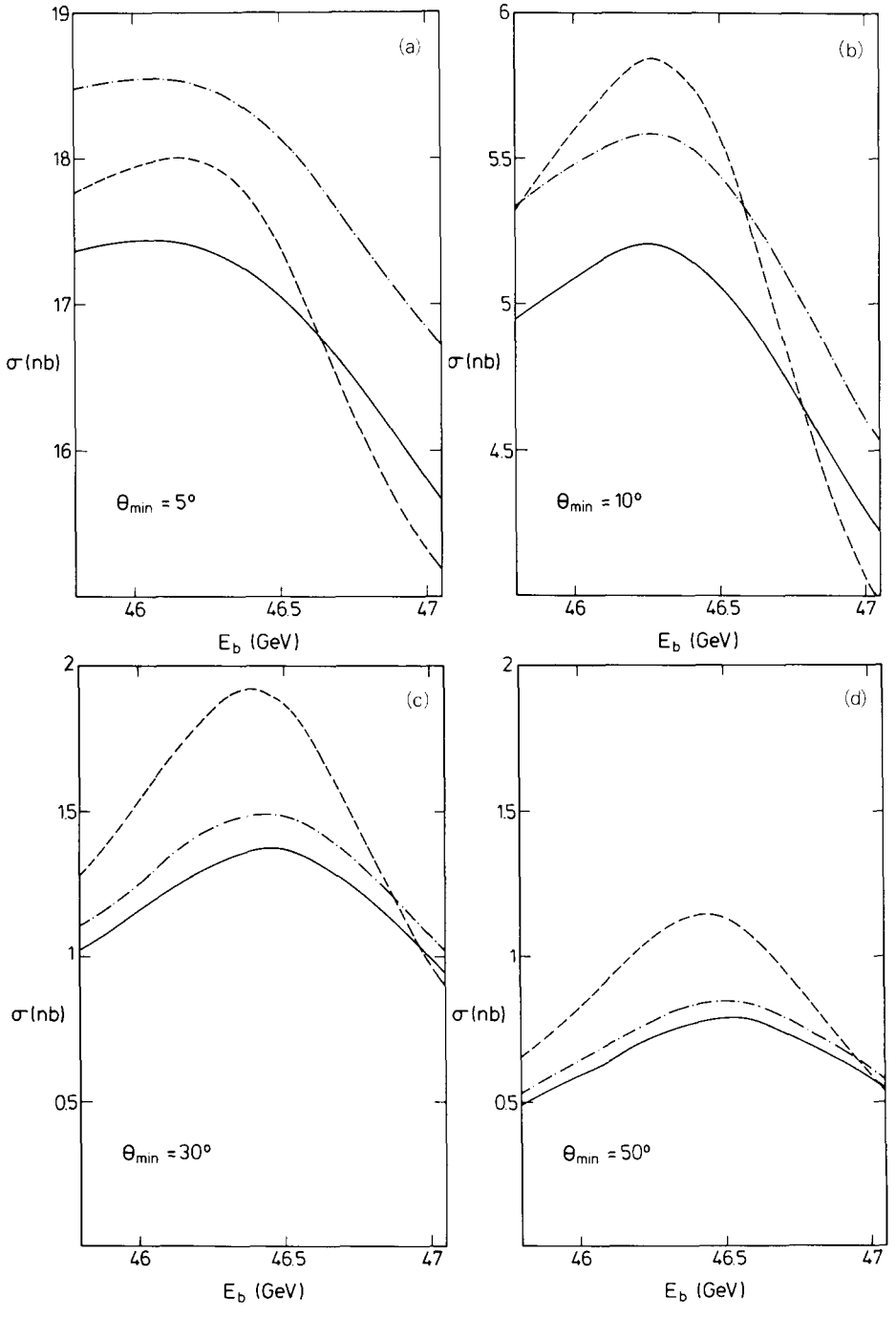

Figs. 4(a)–(d). Resonance shapes of the Z^0 peak with total and canonical corrections, for various angular ranges. Dashed line: lowest order, dashed–dotted line: fully corrected, solid line: result after canonical cuts.

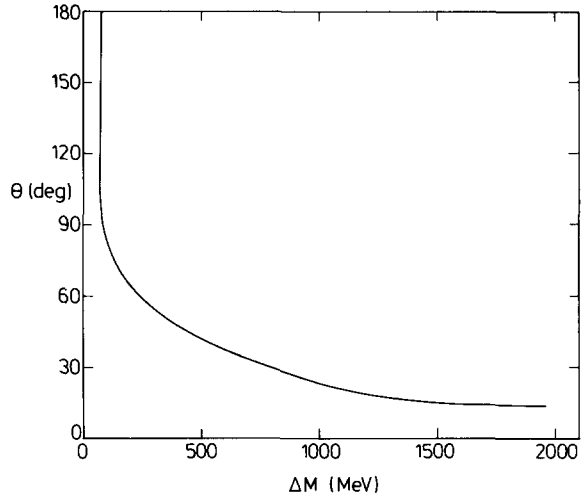

Fig. 5. Apparent mass shift of the Z^0 related to the scattering angle, in the Born approximation.

(dashed-dotted line) and the result after the canonical cuts. As is seen, the cuts serve to lower the resonance curve without affecting its shape. After cuts, the correction also becomes negative again at $\theta_{\min} = 5°$.

A remark is in order on the statistical accuracy of our results. The (statistical) error of course depends on the parameters. It is smallest for $\theta_{\min} = 5°$, being about 0.3% for 10^4 events, and increases to about 0.7% for $\theta_{\min} = 50°$. Of course, this error can be reduced to an arbitrarily small amount by using a sufficiently large number of events. The only possible source of a systematic error can be the particular random-number algorithm; we have found no evidence for any such effect. In figs. 3a–3d, 4c, and 4d the error is of the order of the line widths in the plots, in fig. 4a the error is about 0.05 nb, and in fig. 4b it is about 0.01 nb. It turns out, however, that it is easy to draw a nice smooth curve through the central values, indicating that our error estimates may be quite conservative. In particular, the peak of the resonance curve can be well identified.

This brings us to the next topic of interest; the peak shift. Due to the interference between the Z^0 and photon exchange graphs the peak of the cross section will be shifted from the exact value of $\sqrt{s} = m_Z$ to a value $\sqrt{s} = m_Z - \Delta_m$: Δ_m is the peak shift (*positive* if the peak is at *lower* values than m_Z). The peak shift is present already at the Born level where we can find it with great precision because we know the resonance curve analytically. In fig. 5 we present the relation between Δ_m and the scattering angle θ. The peak shift is always positive: its minimum is about 70 MeV at θ around 100 degrees. For larger values of θ it remains essentially constant. At smaller angles the peak shift increases rapidly; at $\theta = 23°$ it reaches 1 GeV. For $\theta \sim 13°$ ($\Delta_m \sim 1900$ MeV) the effect of the Z^0 resonance becomes sufficiently

TABLE 2
Apparent mass shift of the Z^0 for various angular ranges

Angular range (deg)	Peak shifts (MeV)		
	Born	full correction	canonical
5–175	680	900 ± 100	900 ± 100
10–170	444	460 ± 40	460 ± 40
30–150	214	80 ± 40	70 ± 40
50–130	132	-20 ± 40	-40 ± 40

relatively small that it can no longer compensate the $1/s$ dependence of the photon cross section, and the cross section does not even become flat anymore as a function of $\sqrt{s}$. Determination of the peak shift in the radiatively corrected cross sections is less precise due to the statistical errors. We determined the peak shift both graphically and by fitting to the cross section values at four points in a 300 MeV interval around the resonance. These results typically coincide to about 20–40 MeV which we take as an error estimate. In table 2 we present the peak shifts for the Born, fully corrected and canonically corrected cross sections in the four angular ranges. For $\theta_{\min} = 5°$ and 10° the corrections shift the peak to lower values. In the more central regions the peak shift is reduced by the corrections; for $\theta_{\min} = 50$ the peak actually shifts to values of $\sqrt{s}$ larger than m_Z. Of course, runs with higher statistics can improve the accuracy of these results. We deemed this not relevant at this point because of the extent uncertainties in m_Z. The overall conclusion is clear however: the peak shift is quite substantial and can be given about any value by applying suitable cuts.

The last quantity of interest is the effect of changes in the acollinearity cut ζ. To this end we made a number of runs using 10^5 points at values $E_b = 44$, 46.5 and 49 GeV. The resulting values for the radiative corrections are given in fig. 6. It is seen that the absolute value of the correction depends (of course) on E_b; its variation with ζ is, however, always about the same. Moreover, for ζ smaller than about 10 degrees the correction varies quite rapidly with ζ, implying that measurement errors in the e^+, e^- directions will become important. $\zeta = 10$ degrees seems to be the optimal choice, giving reasonable corrections which are not too sensitive to measurement errors. We finish this section by presenting our conclusions.

First, an optimal choice for $\Delta E/E_b$ is dictated by the process under study; if we restrict ourselves to first-order corrections, $\Delta E/E_b$ must be between 0.7% and 1%.

Second, the total radiative correction is a bit more moderate than in the muon case; at smaller scattering angles it remains positive even at resonance. No high radiative tail is present. As for canonical cuts, an acollinearity cut on the e^+e^- pair works well and a value $\zeta = 10°$ is optimal. After canonical cuts the resonance peak drops in height but keeps the same shape. Finally, we have determined the shifts in

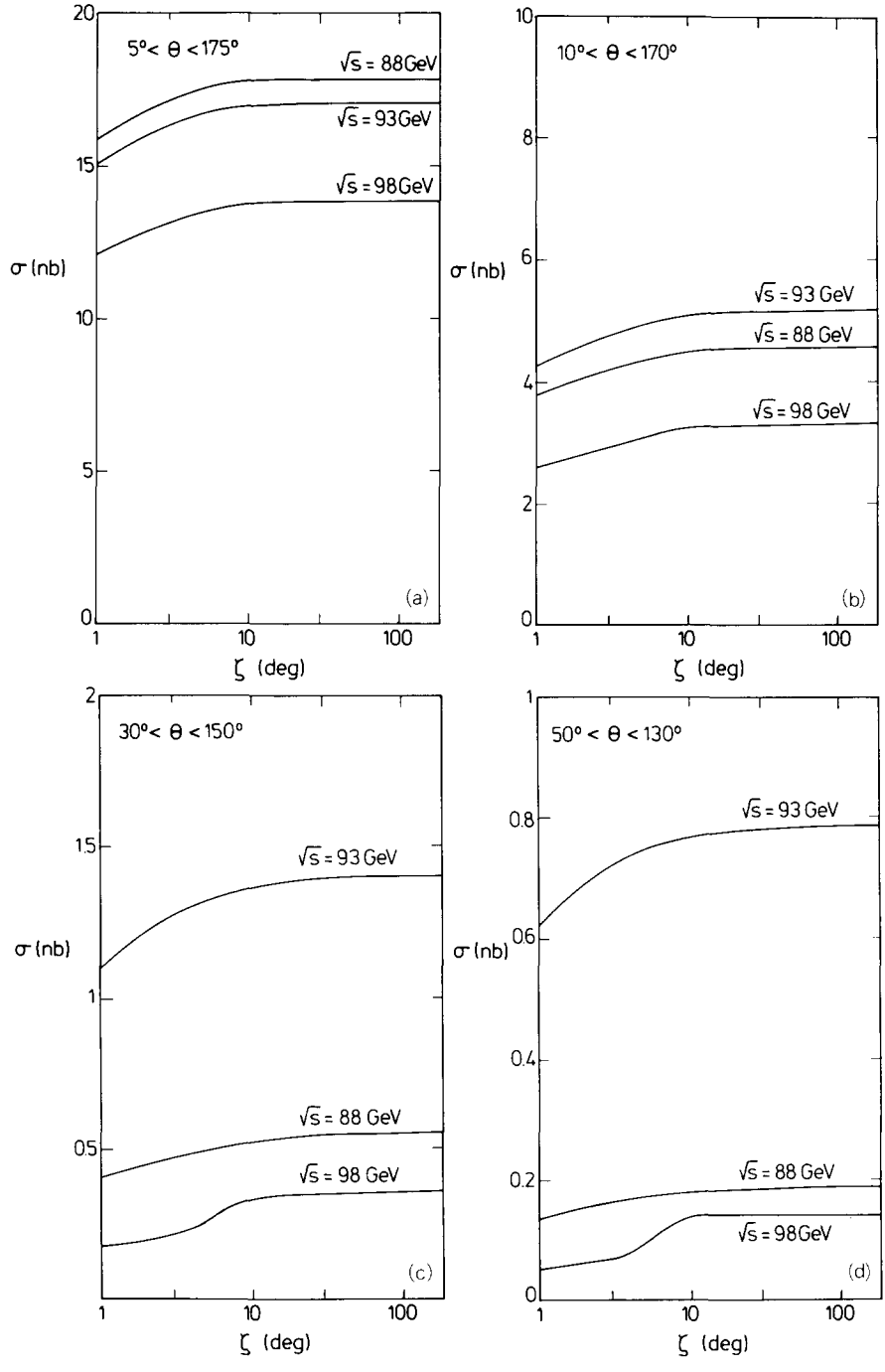

Figs. 6(a)–(d). Dependence of the radiative correction on the value of the acollinearity cut, for various angular ranges.

the apparent Z^0 peak from its exact mass value. This shift is affected considerably by the angular interval considered and by radiative corrections, and to a lesser extent by the application of canonical cuts.

Appendix A

In sect. 2 we gave an expression for the matrix element squared, summed and averaged over the spins. This expression is in terms of spinor products. As stated there, it can be rewritten in a form consisting of only the more conventional vector products, which we shall give below. First, we define two functions of four four-momenta p_1, p_2, p_3 and p_4

$$R(p_1, p_2, p_3, p_4) = 4\{-(k\cdot p_1)(k\cdot p_3)(p_2\cdot p_4) + (k\cdot p_2)(k\cdot p_3)(p_1\cdot p_4) + (k\cdot p_1)(k\cdot p_4)(p_2\cdot p_3) - (k\cdot p_2)(k\cdot p_4)(p_1\cdot p_3)\}, \quad (A.1)$$

$$I(p_1, p_2, p_3, p_4) = 4\{(k\cdot p_1)\varepsilon_{\mu\nu\rho\sigma}p_2^\mu k^\nu p_4^\rho p_3^\sigma - (k\cdot p_2)\varepsilon_{\mu\nu\rho\sigma}p_1^\mu k^\nu p_4^\rho p_3^\sigma\}, \quad (A.2)$$

where k^μ is the four-momenta of the bremsstrahlung photon, and $\varepsilon_{\mu\nu\rho\sigma}$ the Levi–Civita tensor with $\varepsilon_{0123} = +1$. The I has, in fact, the same symmetries in the p_i as R; this is easily proved using Schouten's identities. Next, we have two functions of two kinematic invariants $(s, s', t, \ldots)$

$$Q_{\lambda_1\lambda_2}(x, y) = 8e^2\left[\frac{e^4}{xy} + e^2(v-\lambda_1 a)(v-\lambda_2 a)\left(\frac{y-m_Z^2}{xB(y)} + \frac{x-m_Z^2}{yB(z)}\right) + (v-\lambda_1 a)^2(v-\lambda_2 a)^2\frac{(x-m_Z^2)(y-m_Z^2)+m_Z^2\Gamma_Z^2}{B(x)B(y)}\right], \quad (A.3)$$

$$J_{\lambda_1\lambda_2}(x, y) = 8e^2(v-\lambda_1 a)(v-\lambda_2 a)m_Z\Gamma_Z \times\left[\frac{-e^2}{yB(x)} + \frac{e^2}{xB(y)} + (v-\lambda_1 a)(v-\lambda_2 a)\frac{x-y}{B(x)B(y)}\right], \quad (A.4)$$

where $\lambda_{1,2}$ take on the values $+$ or $-$, and

$$B(x) = (x-m_Z)^2 + m_Z^2\Gamma_Z^2. \quad (A.5)$$

The equivalent expression to eq. (2.1) can then be written as

$$\begin{aligned}
\tfrac{1}{4}\Sigma|M|^2 = \big[&(u^2+u'^2)\{R(q_-q_+q_-q_+)[Q_{++}(s',s')+Q_{--}(s',s')]\\
&+R(p_+p_-p_+p_-)[Q_{++}(s,s)+Q_{--}(s,s)]\\
&+R(q_-p_-q_-p_-)[Q_{++}(t',t')+Q_{--}(t',t')]\\
&+R(p_+q_+p_+q_+)[Q_{++}(t,t)+Q_{--}(t,t)]\\
&+2R(q_-q_+p_+p_-)[Q_{++}(s',s)+Q_{--}(s',s)]\\
&+2R(q_-q_+q_-p_-)[Q_{++}(s',t')+Q_{--}(s',t')]\\
&+2R(q_-q_+p_+q_+)[Q_{++}(s',t)+Q_{--}(s',t)]\\
&+2R(p_+p_-q_-p_-)[Q_{++}(s,t')+Q_{--}(s,t')]\\
&+2R(p_+p_-p_+q_+)[Q_{++}(s,t)+Q_{--}(s,t)]\\
&+2R(q_-p_-p_+q_+)[Q_{++}(t',t)+Q_{--}(t',t)]\}\\
&-2(u^2-u'^2)\{I(q_-q_+p_+p_-)[J_{++}(s',s)-J_{--}(s',s)]\\
&+I(q_-q_+q_-p_-)[J_{++}(s',t')-J_{--}(s',t')]\\
&+I(q_-q_+p_+q_+)[J_{++}(s',t)-J_{--}(s',t)]\\
&+I(p_+p_-q_-p_-)[J_{++}(s,t')-J_{--}(s,t')]\\
&+I(p_+p_-p_+q_+)[J_{++}(s,t)-J_{--}(s,t)]\\
&+I(q_-p_-p_+q_+)[J_{++}(t',t)-J_{--}(t',t)]\}\\
&+2(t^2+t'^2)\{R(q_-q_+q_+q_+)Q_{+-}(s',s')+R(p_+p_-p_+p_-)Q_{+-}(s,s)\\
&\qquad+2R(q_-q_+p_+p_-)Q_{+-}(s',s)\}\\
&+2(s^2+s'^2)\{R(q_-p_-q_-p_-)Q_{+-}(t',t')+R(p_+q_+p_+q_+)Q_{+-}(t,t)\\
&\quad+2R(q_-p_-p_+q_+)Q_{+-}(t',t)\}\big]/64(p_+k)(p_-k)(q_+k)(q_-k).
\end{aligned} \tag{A.6}$$

We have checked both analytically and numerically that this result is identical to the one obtained in sect. 2.

Appendix B

We briefly outline the structure of our Monte Carlo program. The five different channels in which events can be generated are represented by so many "subgenerators", sets of subroutines that operate independently. Our program, therefore, has a modular structure. The initialization of the program is performed by calling the routine SETBAB. To this the user supplies the beam energy, and the masses of the Z^0 and Higgs bosons, and of the top quark. Furthermore, the crude phase space cuts $\theta_{\min}$, $\theta_{\max}$ and $k_{\max}$ are specified, where $k_{\max}$ is the maximum energy one wishes to allow for in units of E_b (for instance, with the canonical cuts described in sect. 8 a value of $k_{\max} = 0.51$ would be appropriate since events with larger photon energy would always be rejected). The initialization program then performs the following tasks; it calculates the Standard Model values of m_w, Γ_Z and $\sin^2\theta_w$; then, it calls five separate initialization routines for the five subgenerators. These return the values of the approximate cross sections σ_i, $i = 1,\ldots,5$. On the basis of these values, and using given a priori probabilities α_i $(i = 1,\ldots,5)$, it computes the relative probabilities of an event to come from each channel*. An actual Monte Carlo event is generated by a call to the generation routine GENBAB. This routine first picks a channel and calls the subgenerator routine for that channel. These routines use the algorithms given in sect. 7 and return the values of q_+^μ, q_-^μ and k^μ, together with the value of W_m. GENBAB first checks whether the event satisfies the restrictions given by $\theta_{\min}$ and $\theta_{\max}$ (the $k_{\max}$ cut is automatically satisfied). If so, the event weight is calculated. For hard photon events the expressions given in sects. 2 and 5 are used, while a soft photon event has constant weight. The weight information is stored in common, while the routine outputs the momenta values and the total weight. Optionally, unweighted events are generated by rejection. Additional cuts (such as canonical ones) have to be implemented by the calling program.

After the desired event sample has been generated, the computation of the cross section corresponding to this sample is performed by routine ENDBAB. This uses the values of σ_i and α_i, and the information on the event weights, to estimate the resultant cross section and the statistical uncertainty. The results are printed in the form of a table in which also information on the performance of the individual subgenerators is given.

We finish this appendix by specifying the random-number generator used in our program. It is a multiplicative congruentional pseudo-random-number generator based on the algorithm

$$k_i = (69069 k_{i-1}) \bmod 2^{31}, \qquad \rho_i = k_i/2^{31}, \tag{B.1}$$

where ρ_i is the current random number, and ρ_{i-1} the previous one. If desired, this

* The results presented in sect. 8 are based on $\alpha_i = 1$.

generator can be replaced by any other one in which the user has confidence; the results should be the same within statistical errors.

Appendix C

We present the Born level formula for the cross section for $e^+e^- \to e^+e^-$, integrated over the complete azimuthal range, and polar angles from $\theta_{\min}$ up to $\theta_{\max}$. To our knowledge this result has not been given anywhere in the literature, and we include it here for completeness. It reads

$$\sigma = \frac{1}{32\pi s}\left[B(\cos\theta_{\min}) - B(\cos\theta_{\max})\right], \tag{C.1}$$

where

$$\begin{aligned} B(c) = {} & 2e^4\phi_1(c) + \left(\sigma_+^2 + \sigma_-^2\right)\phi_2(c) \\ & + \left[(g_v+g_a)^4 + (g_v-g_a)^4\right]\phi_3(c) + 2e^2\mathrm{Re}(\sigma_+ + \sigma_-)\phi_4(c) \\ & + 2\,\mathrm{Re}\left[(g_v+g_a)^2\sigma_+ + (g_v-g_a)^2\sigma_-\right]\phi_5(c) \\ & + 2e^2\left[(g_v+g_a)^2 + (g_v-g_a)^2\right]\phi_6(c) + 2\sigma_x^2\phi_7(c) \\ & + 2s^2e^4\phi_8(c) + 2s^2\left(g_v^2-g_a^2\right)^2\phi_9(c) + 4s^2e^2\left(g_v^2-g_a^2\right)\phi_{10}(c), \end{aligned} \tag{C.2}$$

where

$$\begin{aligned} \sigma_+ &= \frac{e^2}{s} + \frac{(g_v+g_a)^2}{s - m_Z^2 + im_Z\Gamma_Z}, \\ \sigma_- &= \frac{e^2}{s} + \frac{(g_v-g_a)^2}{s - m_Z^2 + im_Z\Gamma_Z}, \\ \sigma_x &= \frac{e^2}{s} + \frac{\left(g_v^2-g_a^2\right)}{s - m_Z^2 + im_Z\Gamma_Z}, \end{aligned} \tag{C.3}$$

and the functions $\phi_i(c)$ are given by

$$\phi_1(c) = \frac{4}{1-c} + 4\ln(1-c) - (1-c),$$

$$\phi_2(c) = \tfrac{1}{4}s^2\left[c + c^2 + \tfrac{1}{3}c^3\right],$$

$$\phi_3(c) = \frac{(2+\mu)^2}{1+\mu-c} + 2(2+\mu)\ln(1+\mu-c) + (1+\mu-c),$$

$$\phi_4(c) = \tfrac{1}{2}s\left[4\ln(1-c) - 4(1-c) + \tfrac{1}{2}(1-c)^2\right],$$

$$\phi_5(c) = \tfrac{1}{2}s\left[(2+\mu)^2\ln(1+\mu-c) - 2(2+\mu)(1+\mu-c) + \tfrac{1}{2}(1+\mu-c)^2\right],$$

$$\phi_6(c) = \frac{1}{m_Z^2}(\phi_5(c) - \phi_4(c)),$$

$$\phi_7(c) = \tfrac{1}{4}s^2\left[c - c^2 + \tfrac{1}{3}c^3\right],$$

$$\phi_8(c) = \frac{4}{s^2(1-c)},$$

$$\phi_9(c) = \frac{4}{s^2(1+\phi-c)},$$

$$\phi_{10}(c) = \frac{4}{\mu s^2}\ln\left(\frac{1+\mu-c}{1-c}\right), \tag{C.4}$$

where μ is given by

$$\mu = 2m_Z^2/s.$$

It should be noted that this formula assumes that a Z^0 exchanged in the t-channel has a propagator proportional to $(t - m_Z^2)$, without imaginary part. This is in accordance with the interpretation of the Z^0 width as a perturbative, Q^2-dependent quantity.

References

[1] S.L. Glashow, Nucl. Phys. 22 (1961) 579;
S. Weinberg, Phys. Rev. Lett. 19 (1967) 1264; Phys. Rev. D5 (1972) 1412;
A. Salam, *in* Elementary particle theory, ed. N. Svartholm (Stockholm, 1968) p. 361
[2] M. Böhm, A. Denner and W. Hollik, Nucl. Phys. B304 (1988) 687
[3] J. Ellis and R. Peccei, Physics at LEP, CERN report 86-02

[4] R. Kleiss and P. Zerwas, to be published
[5] A. Barroso et al., Contribution to LEP 200 ECFA Workshop, CERN-EP/87-70
[6] F.A. Berends, R. Gastmans and T.T. Wu, KUL-TF-79/022, paper submitted to the 1979 International Symposium on Lepton and Photon Interactions at High Energies, 1979, Fermi Lab
[7] F.A. Berends, R. Kleiss, P. de Causmaecker, R. Gastmans, W. Troost and T.T. Wu, Nucl. Phys. B206 (1982) 61
[8] R. Kleiss, Z. Phys. C33 (1987) 433
[9] M. Caffo, R. Gatto and R. Remiddi, Phys. Lett. B173 (1986) 91; Nucl. Phys. B286 (1987) 293;
C. Mana and M. Martinez, Nucl. Phys. B287 (1987) 601;
K. Karlen, Nucl. Phys. B289 (1987) 23
[10] F. James, Rep. Prog. Phys. 43 (1980) 1145
[11] R. Kleiss, Ph.D. thesis, Leiden, 1982;
P.H. Daverveldt, Ph.D. thesis, Leiden, 1985
[12] S. Jadach and B.F.L. Ward, Univ. Tennessee preprint-87-0536;
S. Jadach, MPI-PAE/PTh 6/87
[13] F.A. Berends and R. Kleiss, Nucl. Phys. B177 (1981) 237; B178 (1981) 141
[14] F.A. Berends, R. Kleiss and S. Jadach, Nucl. Phys. B202 (1982) 63
[15] F.A. Berends and R. Kleiss, Nucl. Phys. B228 (1983) 537
[16] L. Devroye, Non-uniform random variate generation (Springer, Berlin, 1986)
[17] F.A. Berends and R. Kleiss, Nucl. Phys. B260 (1985) 32
[18] F. Bloch and A. Nordsieck, Phys. Rev. 52 (1937) 54